JACS
JOURNAL OF THE AMERICAN CHEMICAL SOCIETY

Article

Nitric Oxide-Activated "Dual-Key-One-Lock" Nanoprobe for In Vivo Molecular Imaging and High-Specificity Cancer Therapy

Lili Teng, Guosheng Song, Yongchao Liu, Xiaoyu Han, Zhe Li, Youjuan Wang, Shuangyan Huan, Xiao-Bing Zhang, and Weihong Tan

J. Am. Chem. Soc., **Just Accepted Manuscript** • DOI: 10.1021/jacs.9b05901 • Publication Date (Web): 01 Aug 2019

Nitric Oxide-Activated "Dual-Key-One-Lock" Nanoprobe for *In Vivo* Molecular Imaging and High-Specificity Cancer Therapy

Lili Teng‡, Guosheng Song‡, Yongchao Liu, Xiaoyu Han, Zhe Li, Youjuan Wang, Shuangyan Huan, Xiao-Bing Zhang*, Weihong Tan

Molecular Science and Biomedicine Laboratory (MBL), State Key Laboratory of Chemo/Biosensing and Chemometrics, College of Chemistry and Chemical Engineering, Hunan University, Changsha 410082, P. R. China

KEYWORDS*:* Dual-activated, Ratiometric sensing, Photoacoustic imaging, Cancer therapy

ABSTRACT: Cancer treatments are confounded by severe toxic effects toward patients. To address these issues, activatable nanoprobes have been designed for specific imaging and destruction of cancer cells under the stimulation of specific cancer-associated biomarkers. Most activatable nanoprobes were usually activated by some single-factor stimulation, but this restricts therapeutic specificity between diseased and normal tissue; therefore, multi-factor activation is highly desired. To this end, we herein develop a novel dual-stimuli responsive theranostic nanoprobe for simultaneously activatable cancer imaging and photothermal therapy under the coactivation of "dual-key" stimulation of "nitric

oxide (NO)/acidity", so as to further improve the therapeutic specificity. Specifically, we have integrated a weak electron acceptor (benzo[c]-[1,2,5] thiadiazole-5,6-diamine) into a donor-π-acceptor-π-donor (D-π-A-π-D) type chromophore. When the weak acceptor was oxidized by NO in acidic condition to form stronger acceptor (5H-[1,2,3]Triazolo[4,5-f]-2,1,3-benzothiadiazole), the molecule absorption was significantly increased in near-infrared region, based on the intramolecular charge transfer (ICT) mechanism. Under the "dual-key" stimulation of NO/acidity within the tumor associated with inflammation, the nanoprobe can correspondingly output dual signals for ratiometric photoacoustic and photothermal imaging of cancer *in vivo* and do so with enhanced accuracy and specificity. Our novel nanoprobe exhibited higher photoacoustic signals enhancement under dual-factor activation at 9.8 times that of NO and 132 times that of acidity alone, respectively. Moreover, through such dual activation of NO/acidity, the nanoprobe produces more differentiation of hyperthermia between tumor and normal tissues, to afford satisfactory photothermal therapy with minimizing toxicity side effect. Thus, our work presents a promising strategy for significantly improving the precision and specificity of cancer imaging and therapy.

INTRODUCTION

Currently, most cancer treatments, including chemotherapy, radiotherapy or phototherapy, can cause nonspecific chemotoxicity, radiotoxicity or phototoxicity toward noncancerous tissues and thereby induce severe infection, nausea, vomiting, constipation, diarrhea, neuropathic pain and kidney problems, among others.[1-5] Based on the characteristics of the tumor microenvironment (TME), the last few years have seen the development of activatable nanomaterials designed to provide real-time visualization of physiological conditions and effective cancer treatment.[6-16] Under the stimulation of cancer-specific biomarkers, for example, low pH, hypoxia, or high levels of reactive species, ATP, proteases, H_2S, and glutathione (GSH), those nanomaterials were activated to allow for specific destruction of cancer cells upon near-infrared laser or X-ray irradiation, with reduced side-effect toxicity to normal tissues.[8-10, 12-13, 15, 17-19] However, most activatable nanomaterials were only responsive to single stimulation.[9, 12, 17] Such single-factor activation was usually not robust enough to provide the solid signals required to distinguish the site of cancer lesion from normal tissues, resulting in potential false-positive or false-negative diagnostic and therapeutic outcomes.[10, 20-21] In order to further improve the precise capability of cancer treatments, intelligent nanomaterials that can be activated by the coexistence of multiple

cancer-associated biomarkers are highly desired to boost the specificity of therapeutic treatments. However, there are rare reports about such multi-factor activatable nanoprobe developed for efficient cancer therapy driven by near-infrared laser *in vivo*.

Photoacoustic (PA) imaging, as a noninvasive imaging technique, relies on the ultrasound signals produced by the photothermal expansion of light-absorbing tissues or contrast agent using pulsed laser irradiation.[22-25] Compared with the conventional fluorescence or bioluminescence imaging techniques, PA imaging is able to significantly improve imaging depth and spatial resolution *in vivo,* which is promising for clinical translation.[22, 24, 26-31] Currently, molecular imaging based on the PA probe has been developed for cancer diagnosis and monitoring of treatments.[8-9, 18, 22-23, 26, 28-29, 32] However, most PA probes are compromised by the single-factor activation or single-signal output.[8-9, 24, 26, 33] Consequently, the specificity of PA imaging may be depressed by such single-factor stimulation. Moreover, based on the single-signal output, the accuracy of PA imaging may also be influenced by the variability of imaging depth, probe loading or heterogeneous distribution.[22, 34] In order to overcome the imaging artifacts, it is highly desirable to develop sensitive and biocompatible PA imaging nanoprobe responsive to multi-factor stimulation and able to output ratiometric signals for accurate and specific cancer imaging *in vivo*.

To further improve the cancer theranostic specificity, herein, we have designed a dual-activatable theranostic nanoprobe (DATN) (Figure 1b) for simultaneously activatable cancer imaging and photothermal therapy, under the co-stimulation of “nitric oxide (NO)/acidity”. Elevated level of NO plays important pathological roles in various inflammatory diseases.[22, 35] Because inflammation as a hallmark of tumorigenesis is involved in cancer initiation, invasion and metastasis, and the TME is characteristic with acidity.[36-38] Thus, developing NO/acidity-activatable theranostic nanoprobe with photoacoustic feature is highly promising for precise cancer imaging and therapy. In order to construct DATN, we have synthesized a kind of NO/acidity-responsive donor-π-acceptor-π-donor (D-π-A-π-D) type molecule as responsive moieties and another kind of insensitive molecule as internal reference (Figure 1a). Under the coactivation of NO and acidity, the absorbance of DATN at 680 nm increased, while the absorbance at 950 nm remained constant. Because of the high level of NO and low pH in the TME, DATN specifically turned on its photoacoustic signal for *in vivo* tumor-specific PA imaging and could further achieve dual-activatable photothermal therapy with high specificity *in vivo*, especially for those tumors associated with inflammation. Importantly, such intelligent dual-factor-activated theranostic nanoprobe promises to greatly improve the specificity of cancer imaging and therapy.

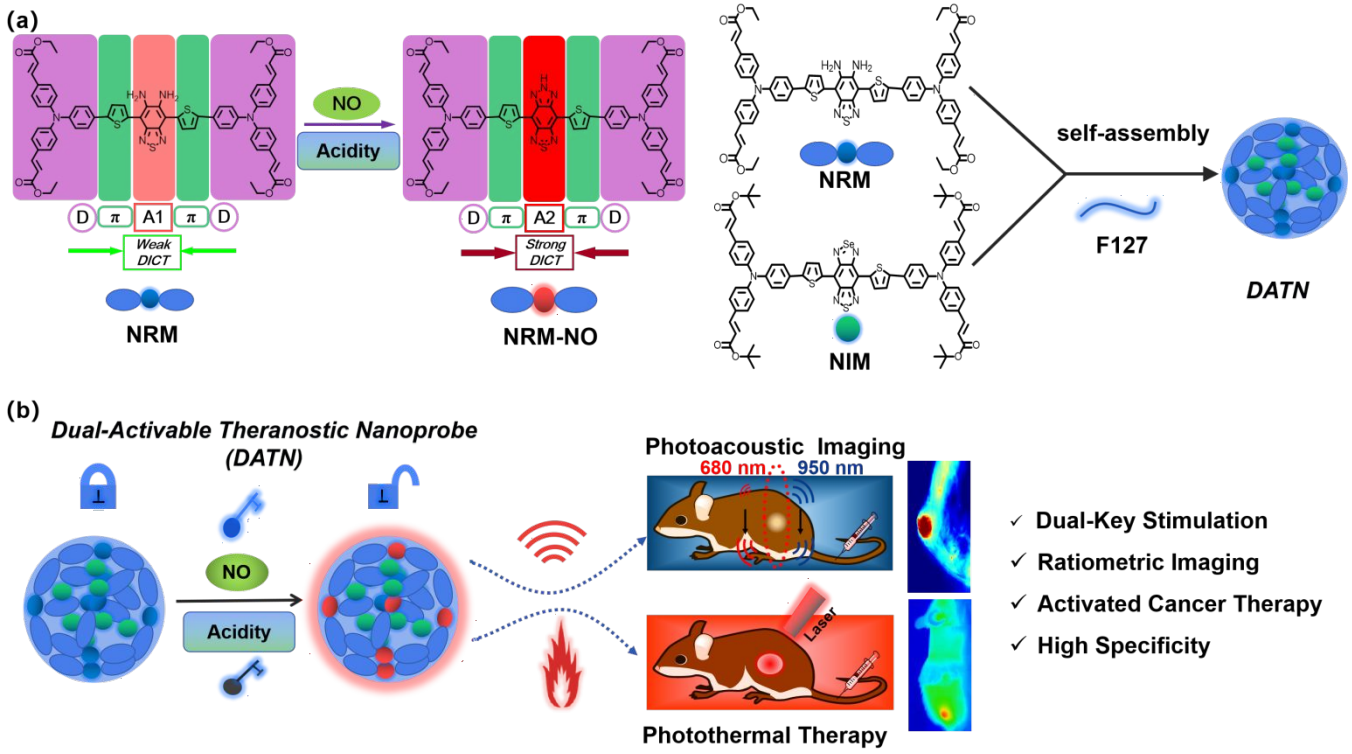

Figure 1. (a) Chemical structures of NRM and NIM used for synthesis of DATN by one-step nanoprecipitation and the illustration of responsive mechanism for NRM to NO and acidity. (b) Scheme showed that under co-activation of NO and acidity within the TME, DATN achieved tumor-specific PA imaging and dual-activatable photothermal therapy.

RESULTS AND DISCUSSION

The Synthetic and Responsive Mechanism of DATN.

First, as shown in Figure 2, we synthesized a NO-responsive molecule (NRM), as responsive moiety and a NO-insensitive molecule (NIM), as internal reference. NRM was designed by integrating benzo[c]-[1,2,5] thiadiazole-5,6-diamine into a D-π-A-π-D chromophore as the weak electron acceptor.[39-40]

Based on the intramolecular charge transfer (ICT) mechanism, when benzo[c]-[1,2,5] thiadiazole-5,6-diamine was oxidized by NO in acidic condition to form a stronger acceptor (5H-[1,2,3]Triazolo[4,5-f]-2,1,3-benzothiadiazole), the absorption of NRM at 600 nm - 750 nm was significantly increased.[39-40] The key steps for assembling the basic structures included Vilsmeier reaction, Witting reaction, Stille-coupling reaction, Suzuki cross-coupling reaction, iron reduction and selenium dioxide (or nitric oxide)-induced ring-closure reaction. Those compounds were characterized by ^{1}H-NMR, ^{13}C NMR, MS, and UV-visible absorption spectra (Figure S1-S23). In order to construct ratiometric theranostic nanoprobe (DATN), we incorporated NRM and NIM into nanoparticle through one-step nanoprecipitation (Figure 1a). After self-assembly of NRM and NIM by Pluronic F127, the resultant DATN showed spherical morphology under transmission electron microscopy (TEM) image (Figure 3a). DATN exhibited good dispersion in H_2O, DPBS, and 1640 cell culture medium with diameters of ~75 nm during 5 days' measurement, as measured by dynamic light scattering (DLS), indicating good colloid stability (Figure 3b, Figure S24). Meanwhile, the Zeta potential of DATN was about - 5.8 mV in water (Figure S25). Under the concurrence of NO and acidity, DATN showed a ratiometric PA signal response. Together with its confirmed photothermal effect, DATN was used for ratiometric photoacoustic /photothermal imaging and dual-activatable cancer photothermal therapy (Figure 1b).

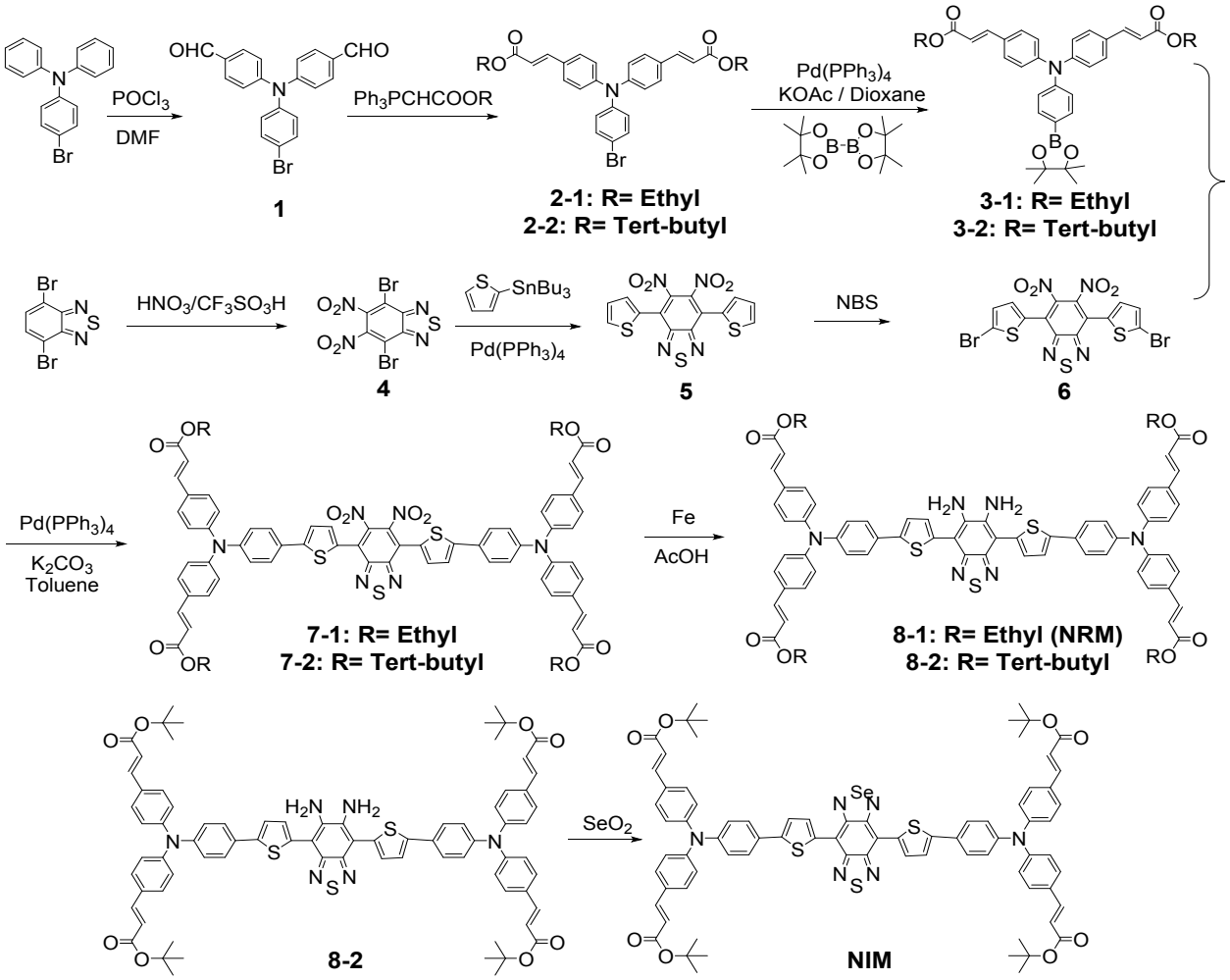

Figure 2. The synthetic route of NRM and NIM.

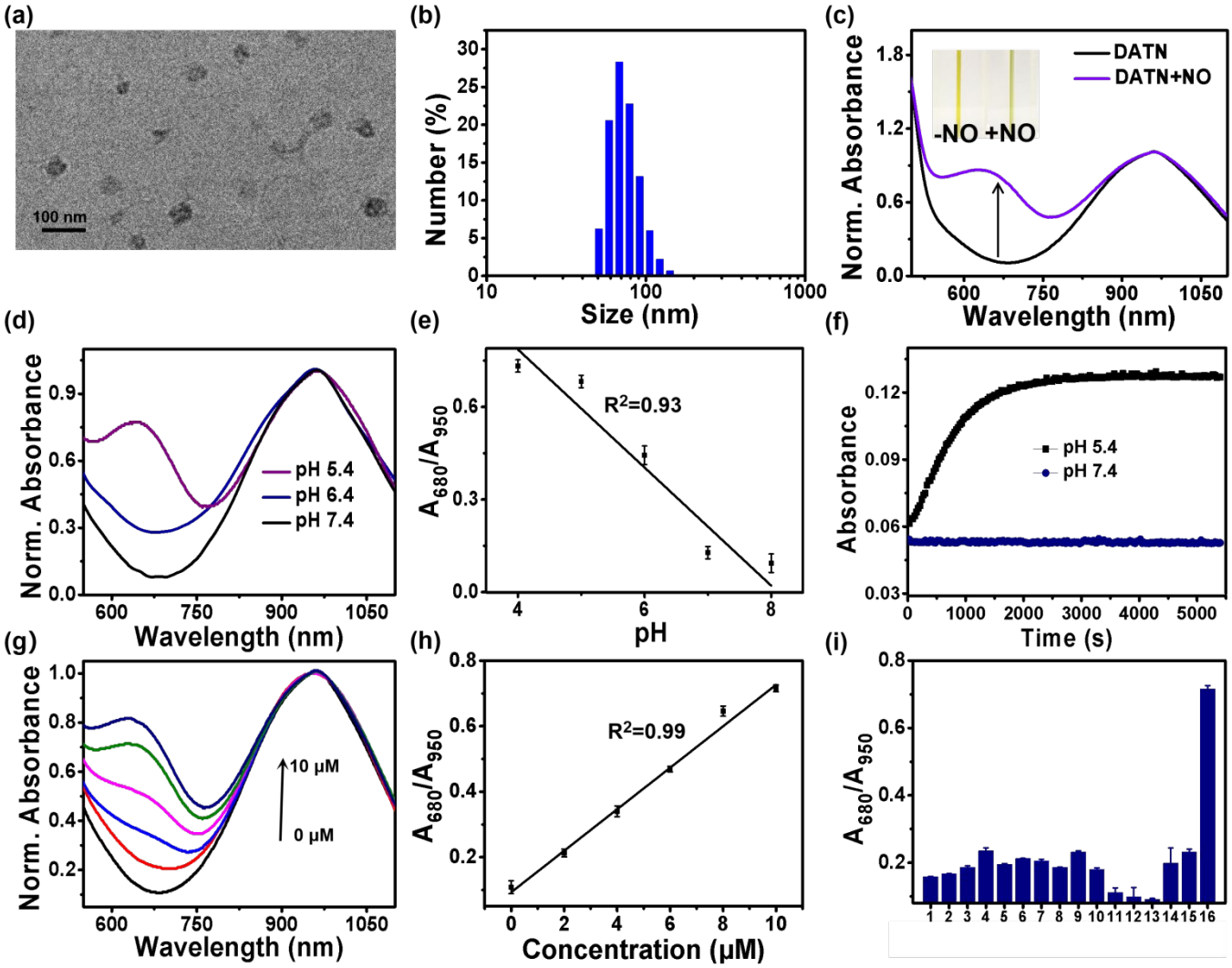

Figure 3. (a) Representative TEM image of DATN. (b) DLS of DATN. (c) The absorbance and photograph of DATN before and after treatment with NO under pH 5.4. (d) Absorbance spectra of DATN (10 μg/mL) in the presence of NO (100 μM) under different pH condition. (e) A_{680}/A_{950} of DATN (20 μg/mL) in the presence of NO (70 μM) under different pH condition. (f) Absorbance of DATN at 680 nm responsive to NO (100 μM) for different time under pH 5.4 and 7.4, respectively. (g) Absorbance spectra of DATN (15 μg/mL) responsive to different concentrations of NO. (h) Plot of A_{680}/A_{950} ratio of DATN to NO concentration. (i) A_{680}/A_{950} responses of DATN (20 μg/mL) incubated with GSH (1 mM), H_2O_2 (500 μM), H_2S_2 (500 μM), ClO^- (50 μM), Hcy (500 μM), HSO_3^- (1 mM), SO_3^{2-} (10 mM),

$O_2^{\cdot-}$ (100 μM), $ONOO^-$ (50 μM), t-BuOOH (100 μM), Cys (500 μM), Fe^{2+} (500 μM), H_2S (500 μM), ·OH (100 μM), Fe^{3+} (500 μM), NO (12 μM). (pH = 5.4).

Detection of NO with DATN.

To confirm the use of using NIM as internal reference for ratiometric PA imaging for NO detection, we first studied the response of NIM toward pH and NO, and we found that different pH values and NO concentrations produced little, to no, effect on the absorbance of NIM (950 nm) at the tested condition (Figure S26). Interestingly, we found that after incubation with buffer solution containing NO (pH = 5.4), we found that the color of DATN solution gradually changed from yellow to green and that the absorbance at 600 nm - 750 nm increased, indicating the good response of DATN to NO in acidic condition (Figure 3c). Next, we investigated the response of DATN toward NO (100 μM) at different pH values. DATN showed remarkable response under pH 5.4, while nearly no response under pH 7.4 (Figure 3d). Moreover, the absorbance ratio of DATN at 680 nm/950 nm (abbreviated as A_{680}/A_{950}) was linear to the pH value with NO (70 μM) in solution (R^2 = 0.93) (Figure 3e). The reaction kinetics of DATN toward NO showed that absorbance of 680 nm reached a plateau within 35 min (Figure 3f) at pH 5.4, but nearly no response at pH 7.4. Thus, we tested the responsivity of DATN toward NO in acidic environment (pH = 5.4). The absorbance of 680 nm gradually enhanced as the concentration of NO

increased, while the absorbance of 950 nm showed no changes (Figure 3g), indicating a dose-dependent responsivity toward NO. Moreover, the A_{680}/A_{950} of DATN showed a good linear correlation (R^2 = 0.99) toward NO concentration between (0 - 10 μM) under pH = 5.4 (Figure 3h). When NO concentration increased to 12 μM, A_{680}/A_{950} reached a plateau (Figure S27). Importantly, the responsive limit (3σ/slope) of DATN for NO was calculated to be 0.326 μM. We further tested the selectivity of DATN, and we found that the A_{680}/A_{950} values presented no obvious enhancement after incubation with a variety of indicated species other than NO under pH = 5.4, indicating the high selectivity of DATN toward NO under acidity (Figure 3i). Thus, the high sensitivity and specificity of DATN could allow for accurate sensing of NO in acidic condition, which is promising for imaging cancers associated with inflammations characterized by an elevated level of NO and lower pH.

Photothermal Responsivity of DATN to NO and Acidity.

Inspired by the high sensitivity and selectivity of DATN, we further studied the photothermal responsivity of DATN to NO at different pH values. In presence of buffer solution (pH = 5.4, 25 μM of NO), DATN could be rapidly heated by 27.3 ℃ and showed dose-dependent temperature increase under the irradiation of 660 nm laser within 5 min (Figure 4a). To compare, with the treatment of corresponding NO (25 μM of NO), the temperature of DATN showed a slight

temperature increase (1.1 ℃) at pH 7.4 under the irradiation of 660 nm laser, and little temperature change (0.7 ℃) at pH 5.4 under irradiation of 980 nm laser (Figure 4b, S28). Thus, the photothermal effect of DATN showed good response with the coactivation of NO and acidity under the irradiation of 660 nm laser. Interestingly, from the photothermal images, temperature was found to rise steeply under 660 nm laser excitation, while under 980 nm laser excitation for 4 min in the presence of various concentrations of NO, no obvious temperature change was noted (Figure 4c). Calculated from Figure 4c, the temperature change ratio of DATN at 660 nm/980 nm (abbreviated as T_{660}/T_{980}) was increased as NO concentration increased. Moreover, we found that the activation by dual factors (pH = 5.4, 25 μM of NO) could raise higher temperature compared to that by the single-factor condition of only NO (pH = 7.4, 25 μM of NO) or only acidity (pH = 5.4, 0 μM of NO), which is promising for highly specific photothermal imaging and photothermal therapy (Figure 4e). The reversible temperature increases also indicated the excellent photothermal stability of activated DATN, even after four times of heating-cooling cycles under irradiation of 660 nm and 980 nm laser (Figure 4f, Figure S29). Besides, the photothermal conversion efficiency of the activated DATN was calculated to be 35.0 %, under irradiation of 660 nm of laser (0.8 W/cm^2) (Figure S30).

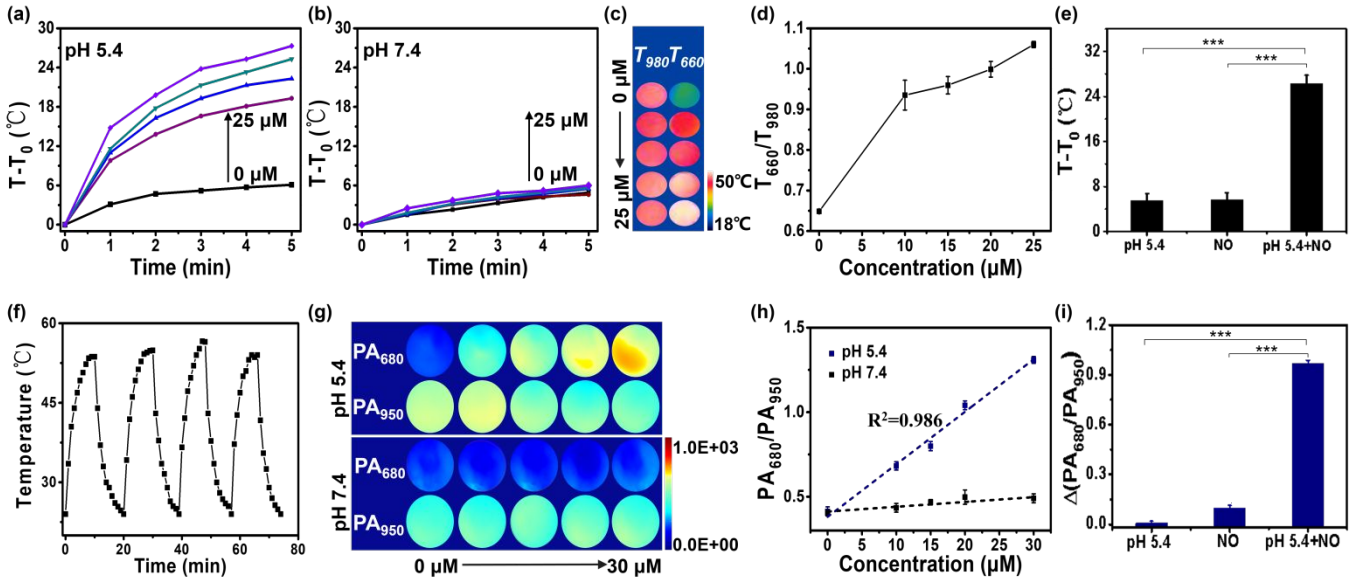

Figure 4. Photothermal response of DATN (25 μg/mL) toward different concentrations of NO under (a) pH 5.4 and (b) pH 7.4, respectively under the irradiation of 660 nm laser. (c) Photothermal images of DATN in the presence of various concentrations of NO. (d) Plot of T_{660}/T_{980} against NO concentrations (pH = 5.4). (e) Photothermal response of DATN toward different conditions, (***p<0.001). (f) Reversible heating-cooling operation of DATN in the presence of NO (25 μM) at pH 5.4, under 660 nm laser irradiation. (g) PA images of DATN (25 μg/mL) toward different concentrations of NO. (h) Plot of PA_{680}/PA_{950} of DATN against NO concentrations. (i) PA_{680}/PA_{950} of DATN responsive toward different conditions, (***p<0.001).

Photoacoustic Responsivity of DATN to NO and Acidity.

We firstly measured the photoacoustic spectra for DATN before and after activation of NO / acidity, and found that the changes of photoacoustic spectra were consistent to that of absorption (Figure S31). We further tested the photoacoustic responsivity of DATN to NO at different pH values. At pH 5.4, the

photoacoustic images showed that the PA signals of DATN from 680 nm excitation were significantly elevated, as the concentration of NO increased, while the PA signals from 950 nm nearly remained constant, indicating the good ratiometric response PA signals toward NO. In comparison, at pH 7.4, both PA signals from 680 and 950 nm showed slight changes in response to NO (Figure 4g). Calculated from Figure 4g, the ratio of DATN's PA signals ratio under excitation of 680 nm/950 nm (abbreviated as PA_{680}/PA_{950}) was linear to NO concentration from 0 to 30 μM (R^2 = 0.986) and the slop at pH 5.4 was higher than that of pH 7.4, indicating DATN possessed better ratiometric PA imaging responsive to NO under acidic condition (Figure 4h). Furthermore, the photoacoustic imaging further confirmed the high selectivity of DATN toward NO in acidity (Figure S32). Moreover, the dual factors (pH = 5.4, 30 μM of NO) were able to trigger higher PA_{680}/PA_{950}, compared to that by the single factor of only NO (pH = 7.4, 30 μM of NO) or only acidity (pH = 5.4, 0 μM of NO), indicating, in turn, that such dual-activatable ratiometric PA imaging may provide higher specificity for cancer imaging (Figure 4i). Besides, the constant photoacoustic signals and corresponding ratios indicated the high photoacoustic stability, during 15 runs' measurement (Figure S33).

Photoacoustic Sensing of NO *In Vivo*.

As a result of the excellent photoacoustic responsivity of DATN to NO in aqueous solution, we further investigated the photoacoustic imaging of NO *in vivo. Before* turning to a lipopolysaccharide (LPS)-induced inflammation model,[22] we assess the background signals from LPS induced inflammation model, and found no obvious interference of photoacoustic signals from LPS (Figure S34). Next, the left and right thighs of mice were pretreated with LPS (3 mg/kg, intramuscular (i.m.) injection) and saline, respectively. The PA images were recorded at 680 nm and 950 nm at different time points post i.m. injection of DATN. As shown in Figure 5a, the left thigh treated with LPS showed stronger PA intensity at 680 nm than the right thigh treated with saline. Notably, calculated from Figure 5a, PA_{680}/PA_{950} ratios of the left thigh were higher than those of the right thigh both at 30 min and 60 min post administration of DATN, indicating that DATN could sensitively monitor the LPS-induced NO generation under acidic condition *in vivo,* using ratiometric PA imaging (Figure 5b). We further investigated the photoacoustic imaging ability of NO within tumor *in vivo* by the DATN. Mice bearing subcutaneous (s.c.) 4T1 xenograft tumor model were injected with DATN (intravenous (i.v.) injection, 10 mg/kg). The PA images were recorded at 680 nm and 950 nm as indicated times (Figure 5c). We found that the contrast of tumor areas was gradually enhanced at excitation of both 680 nm and 950 nm over time, indicating that DATN could efficiently accumulate in the tumor region. Calculated from Figure 5c, the PA signal of tumor areas at 680 nm

showed quicker increase than the signal at 950 nm over time (Figure 5d), which could be attributed to the good responsivity at 680 nm toward NO than that at 950 nm. Notably, PA_{680}/PA_{950} ratios exhibited a gradual increase from 1 h to 5 h, indicating that the ratiometric imaging of DATN could achieve the detection of endogenous NO within the TME *in vivo* (Figure 5e). Besides, strong PA signal from DATN could be observed through 8 mm of tissue, indicating the tissue penetration is suitable for in vivo imaging of mice (Figure S35).

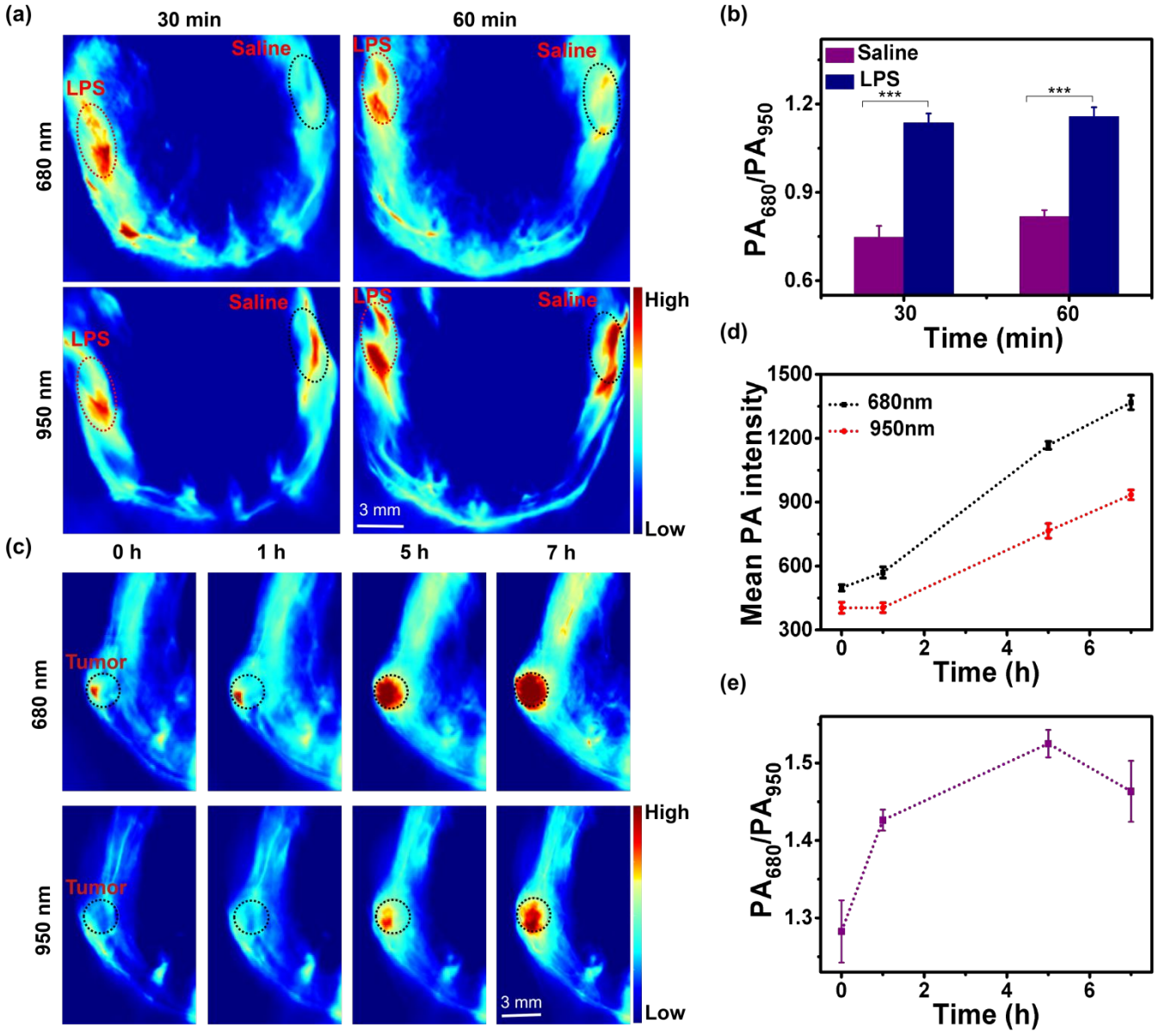

Figure 5. (a) PA images of LPS-stimulated NO. The left and right thighs of mice were intramuscularly injected with LPS or saline, and then injected with PBS buffer containing DATN. (b) The corresponding PA_{680}/PA_{950} ratios, (***$p<0.001$). (c) PA images of endogenous NO within tumor. Mice bearing s.c. 4T1 xenograft tumor was i. v. injected with DATN. (d) PA signal of marked tumor areas. (e) The corresponding PA_{680}/PA_{950} ratios.

Photothermal Imaging of NO within Tumor *In Vivo*.

Apart from the ratiometric PA imaging, DATN was further utilized for photothermal imaging of endogenous NO within tumor *in vivo*. First, mice bearing s.c. 4T1 xenograft tumor received DATN treatment (30 μL, 2 mg/mL) by intratumoral (i.t.) injection into tumor and i.m. injection into left thigh, respectively, and then irradiation of 660 nm laser (1 W/cm^2) at 7 h post treatment. From the thermal images, the tumor displayed quicker temperature increase than the left thigh, suggesting the good photothermal response of DATN toward the TME *in vivo* (Figure S36). Next, we tested the imaging ability of DATN by systematic administration. Mice bearing s.c. 4T1 xenograft tumors received the following treatments: PBS, DATN (i.v. injection, 15 mg/kg), and DATN (i.v. injection, 15 mg/kg) followed by LPS (i.t. injection at 4 h post DATN administration, 3 mg/kg). Seven hours post treatment, thermal imaging was recorded by an IR thermal camera during 660 nm (1 W/cm^2) and 980 nm (0.8 W/cm^2) laser irradiation, respectively (Figure 6a). The tumors treated with DATN and DATN + LPS displayed a rapid temperature increased by 21.3 ℃ and 26.5 ℃ within 4 min, respectively, which was higher than increases noted with PBS treatment under 660 nm laser irradiation (Figure 6b). Thus, LPS could further increase NO levels from TME and thereby enhance temperature responsivity of tumor to 660 nm laser irradiation. We further calculated the temperature change ratio of tumor areas at 660 nm/980 nm (abbreviated as T_{660}/T_{980}) from photothermal images (Figure 6a) and found that the tumor treated with DATN + LPS showed higher

T_{660}/T_{980}, compared with that of tumor treated with DATN, indicating the effective ratiometric detection of inflammation induced NO *in vivo* using photothermal imaging (Figure 6c). Importantly, we found that the tumor (marked areas) treated with DATN + LPS showed the greater temperature difference from normal tissue (marked areas) than that treated with DATN only (Figure 6d), demonstrating that the tumor associated with inflammation could produce more differentiation of hyperthermia of DATN.

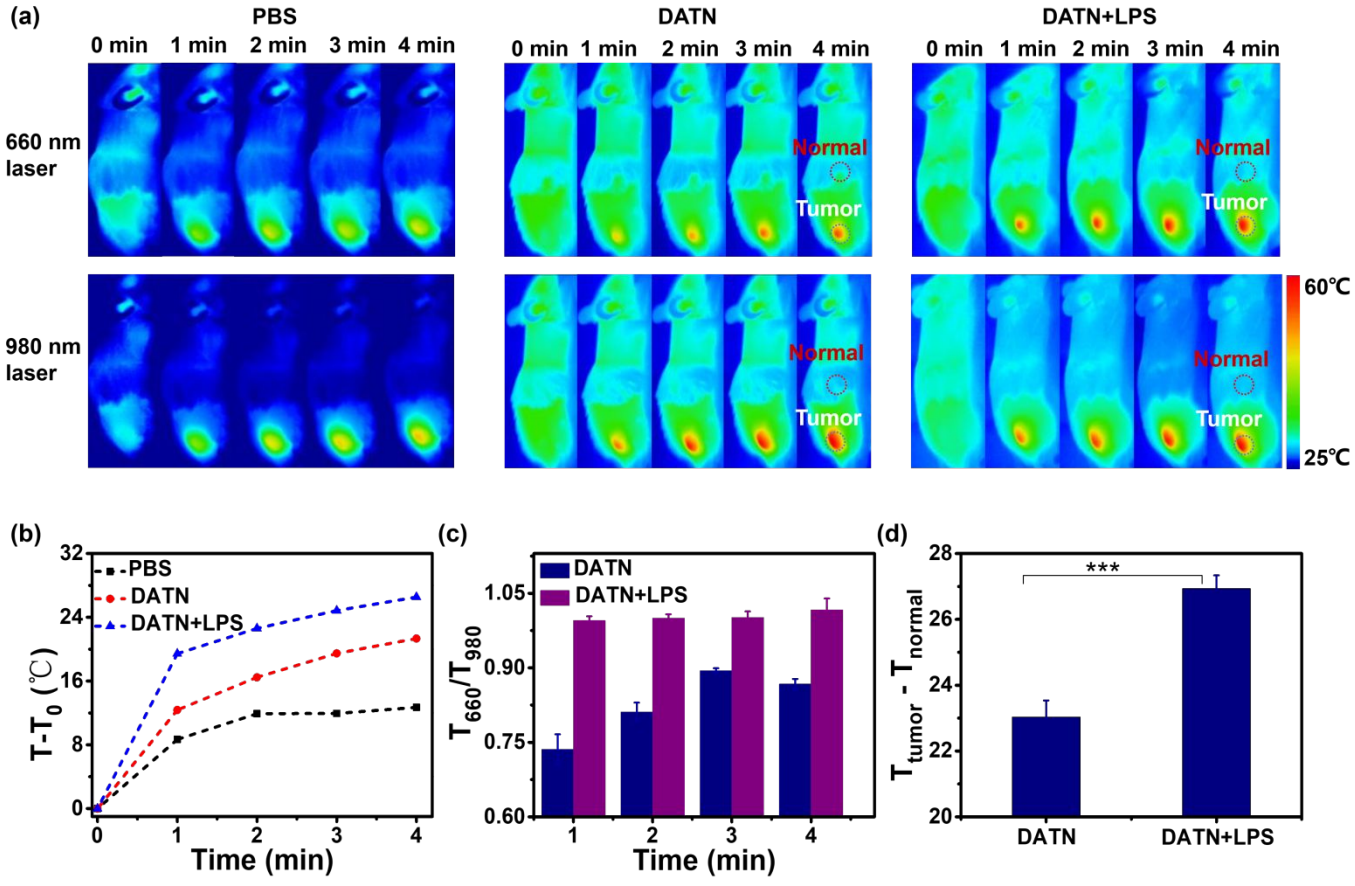

Figure 6. (a) Photothermal images of mice under irradiation of 660 nm and 980 nm laser at 7 h post injection. (b) The representative temperature changes of tumor areas under excitation of 660 nm laser. (c) T_{660}/T_{980} ratio of tumor areas calculated from photothermal images (a). (d) The temperature difference

between marked tumor and normal tissue at 4 min under irradiation of 660 nm laser, calculated from (a), (***p<0.001).

NO/Acidity Activatable Photothermal Cancer Treatment.

As a photothermal and photoacoustic nanoprobe applied for *in vivo* imaging, DATN should possess low cytotoxicity. We investigated the cytotoxicity of DATN by a standard MTS assay toward various cell lines: mouse breast carcinoma (4T1) cells, human cervical carcinoma (HeLa) cells, and human embryonic kidney (HEK293) cells. We found that DATN produced nearly no effect on the cell viability of both malignant cancer cell lines and normal cell lines, even under the incubation of high concentration (80 μg/mL) for 24 h, indicating its minimal cytotoxicity (Figure S37). Considering the excellent photothermal/photoacoustic response and high biocompability, we further promoted DATN as a NO/acidity-activated photothermal agent for cancer treatment. In order to present the therapeutic effect of DATN, mice bearing s.c. 4T1 xenograft tumor were divided into five groups: (I) PBS; (II) only DATN; (III) only laser irradiation; (IV) DATN + laser; (V) DATN + LPS (3 mg/kg, i.t. injection at 4 h after DATN administration) + laser. These mice were i.v. injected with DATN (15 mg/kg) and received 660 nm laser irradiation (1 W/cm^2, 15 min) at 7 h post injection. From the tumor growth curves and tumor weights at the fifteen days post treatment, we found that the tumor treated with DATN + laser showed considerable suppression compared with that treated with only DATN or only laser, indicating the good photothermal

therapeutic effect of DATN activated by endogenous NO (Figure 7a, b). In order to further enhance the treatment efficacy, LPS was used to elevate NO level within tumor to, in turn, enhance the photothermal effect of DATN. The immunohistochemical staining image of tumor slice confirmed the real existing severe inflammation within tumor induced by LPS (Figure S38). As expected, after LPS treatment, the tumor exhibited higher tumor inhibition, compared with that treated with group IV. Furthermore, the histological hematoxylin and eosin (H&E) staining results clearly revealed that the tumors treated with DATN + LPS + laser had much more necrotic areas than that of other groups under the same laser irradiation (Figure 7d). These results suggested that NO/acidity activatable photothermal effect of DATN could significantly inhibit the tumor growth, especially for those tumors with severe inflammation. Moreover, those mice showed no obvious loss of body weight for all groups during 15 days after photothermal therapy (Figure 7c). In addition, H&E staining of major organs from each group also exhibited no noticeable pathological changes after treatment (Figure 7e), suggesting the low side effects of DATN for such photothermal therapy. These results clearly indicated that DATN could be effectively triggered for photothermal ablation of tumor under the activation of inflammation-induced NO and acidic TME.

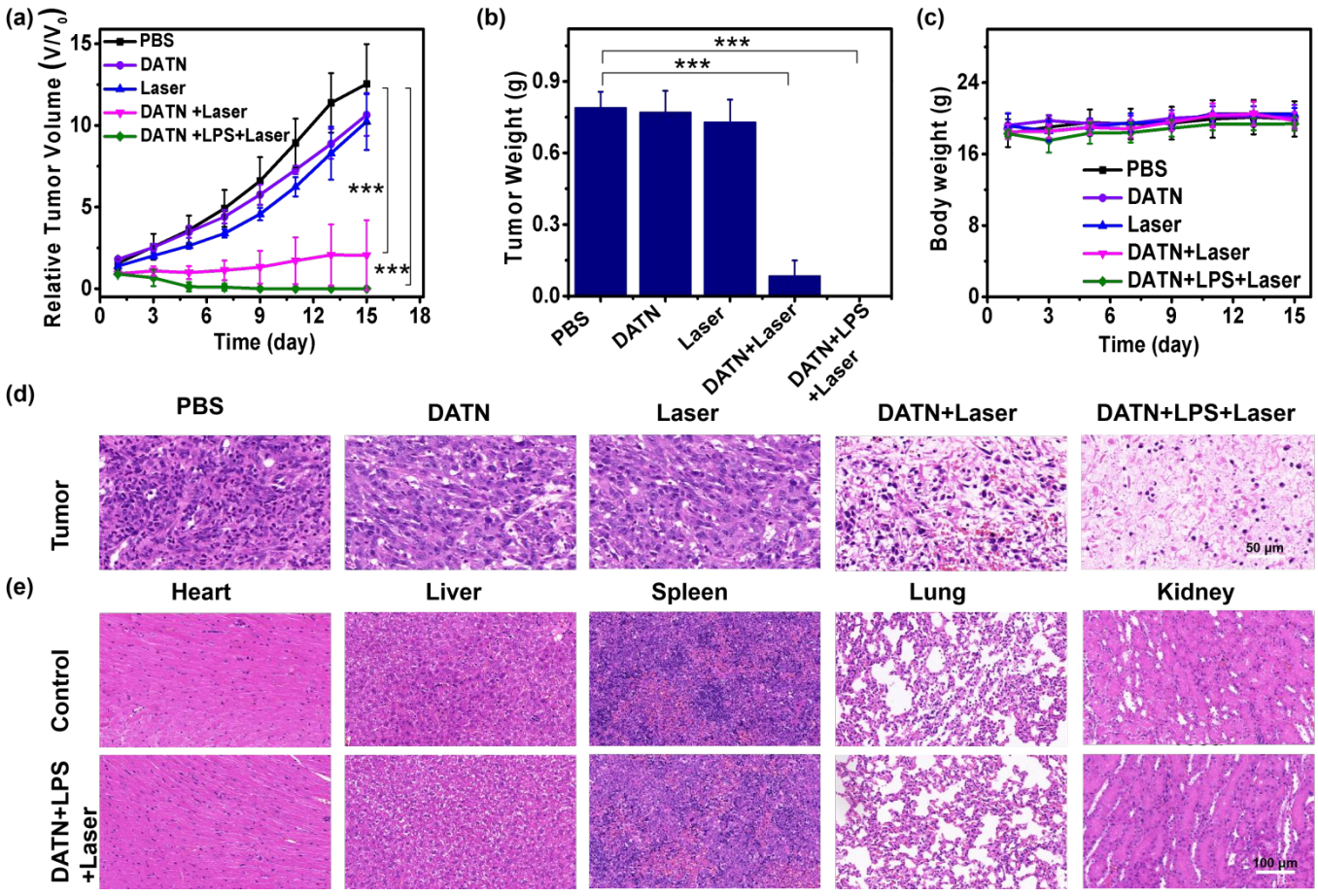

Figure 7. *In vivo* cancer treatment of DATN. (a) Tumor growth curves, (***p<0.001). (b) Tumor weights of each group at the fifteen days post irradiation, (***p<0.001). (c) Body weights of each group. (d) Representative H&E-stained tumor slices of each group on the second day post irradiation. (e) Representative H&E-stained major organs from groups (I) and (V) group at the fifteen days post irradiation.

In TME, single-factor activatable probes were typically compromised by the poor signal to noise ratio and "false positive" results for specific cancer imaging. In this study, we have developed a “two-key-one-lock” ratiometric imaging nanoprobe with the good sensitivity and selectivity toward NO at acidic condition.

Because the acidity and NO are characteristics of tumors associated with inflammation, the nanoprobes could be activated through the coexistence of these two factors for the photothermal/photoacoustic imaging of tumors, which was superior to single-factor activation. Specifically, DATN exhibited higher photoacoustic signals enhancement under dual-factor activation, specifically, 9.8 times that of NO and 132 times that of acidity alone, respectively. Moreover, those PA signal from 680 nm and 950 nm could be used for ratiometric imaging in order to overcome the interference from the probe's concentration, depth and heterogeneous distribution. Importantly, the combination of photoacoustic and photothermal imaging allowed for more accurate imaging diagnosis. In this theranostic nanoprobe, DATN could be heated by 27.3 ° C through dual-factor activation, but only heated by about 6 ° C by single factor such as NO or acidity. Thus, the photothermal efficacy of DATN could be greatly enhanced, but only under the coexisting NO and acidity, making the nanoprobe suitable for highly specific cancer therapy. Furthermore, a better therapeutic outcome would be achieved for the tumors associated with severe inflammation, as a consequence of high level of NO. Such dual-factor activation could largely reduce the phototoxicity to normal tissues in comparison with the single-factor activation.

CONCLUSIONS

We have elaborately developed a novel dual-factor activatable theranostic nanoprobe for ratiometric photoacoustic/photothermal imaging and activatable cancer therapy. With the coactivation of NO/acidity within TME, DATN could turn on its ratiometric photoacoustic signals for tumor-specific photoacoustic imaging *in vivo*. Moreover, DATN achieved dual-activatable photothermal therapy with higher tumor-specificity and good biocompatibility *in vivo*, especially for cancers associated with inflammation. Such multi-factor activatable strategy is promising for greatly reducing the severe toxic effects of cancer treatments. Our continuing experiments include the development of a longer-wavelength photothermal agent to achieve deeper tumor treatment by changing the molecular skeleton and the employment of more specific cancer biomarkers, e.g., matrix metalloproteinases, to further improve the specificity of cancer imaging and therapy.

EXPERIMENTAL SECTION

Materials and Characterization. All reagents and chemicals were obtained from commercial suppliers. Ultrapure water was utilized from a Milli-Q reference system (Millipore). Reactive oxygen/nitrogen species were prepared according to the previously reported literature.[39, 41] Reagents for cell culture were supplied by Gibco (Tulsa, OK, U.S.A.). Transmission electron microscope images were accomplished using JEM-2100F (JEOL). Dynamic light scattering (DLS) measurements were made on a Malvern Zetasizer Nano ZS90 (Malvern). The

absorbance was recorded by ultraviolet-visible absorption spectrometry (UV-1800, Shimadzu) or microplate reader (SpectraMax iD3). Mass spectra were recorded in an LCQ advantage ion trap mass spectrometer (Thermo Finnigan). NMR spectra were measured with a Bruker-400 spectrometer. All photoacoustic images were analyzed and collected at various time points by InVision 256-TF imaging system (iTheraMedical, Germany). Photothermal images were recorded by an IR thermal camera (FLIR Systems, Inc.). All animal experiments were performed in compliance with the relevant laws and approved *by the Institutional Animal Care and Use Committee* of Hunan University.

Preparation of Nanoprobe (DATN). A tetrahydrofuran (THF) solution (2 mL) containing NRM (0.5 mg), NIM (0.5 mg) and Pluronic F127 (4 mg) was rapidly injected into distilled-deionized water (5 mL) under sonication. After sonication for another 4 min, the solution was evaporated at 45 °C by rotary evaporation to remove excess THF. Finally, the DATN solution was purified by ultrafiltration (50 K, 4,000 r.p.m) for several times. The final concentration of DATN was determined by the concentration of NRM.

Cell Cytotoxicity. Mouse breast carcinoma (4T1) cells, human cervical carcinoma (HeLa) cells, and human embryonic kidney (HEK293) cells were cultured in Dulbecco's Modified Eagle's medium (DMEM) supplemented with

10% fetal bovine serum (FBS) and 1 % antibiotics (penicillin-streptomycin) at 37 °C with 5 % CO_2. Cells were seeded at a density of 1 × 10^4 cells per well in 96-well plates and cultured for 12 h under the above conditions. Then, the culture medium was replaced, and the cells were exposed to different concentrations of DATN (0-80 μg/mL) for another 24 h. Finally, cell viabilities were detected by a standard MTS assay.

Tumor Imaging *In Vivo*. To develop the s.c. tumor model, 4T1 cells (1 × 10^6) suspended in 25 μL of PBS were s.c. injected into the back of each mouse (5-6 weeks, female). For *in vivo* PA imaging, the left and right thighs of mice were pretreated with lipopolysaccharide (LPS) (3 mg/kg, i.m. injection) and saline, respectively. The PA images were recorded at 680 nm and 950 nm at indicated time points post-i.m. injection of PBS solution containing DATN (50 μL, 300 μg/mL, pH = 5.4) (excitation wavelengths at 680 and 950 nm). Mice were then anesthetized by isoflurane in oxygen during PA imaging. For *in vivo* PA imaging of tumor, mice bearing s.c. 4T1 xenograft tumor were i.v. injected with DATN (100 μL, 10 mg/kg) and anesthetized for PA imaging (excitation wavelengths at 680 and 950 nm). For *in vivo* photothermal imaging, mice bearing 4T1 tumors were divided into three groups: (i) PBS (i.v. injection, 150 μL), (ii) DATN (i.v. injection, 150 μL, 15 mg/kg) and laser irradiation, and (iii) DATN (i.v. injection, 150 μL, 15 mg/kg) + LPS (3 mg/kg, i. t. injection at 4 h after DATN

administration) + laser irradiation. 7 h after injection, the mice received 660 nm (1 W/cm^2) or 980 nm (0.8 W/cm^2) laser irradiation. The irradiation area was 0.8 cm^2. An IR thermal camera was used to monitor the temperature changes of the tumors using an IR thermal camera during laser irradiation.

***In Vivo* Photothermal Therapy.** For *in vivo* photothermal therapy, mice bearing 4T1 tumors were divided into five groups (n = 4 per group): (I) PBS; (II) only DATN; (III) only laser irradiation; (IV) DATN + laser irradiation; and (V) DATN + LPS (3 mg/kg, i.t. injection at 4 h post DATN administration) + laser irradiation. Mice from Group II, IV, V were i.v. injected DATN (150 μL, 15 mg/kg). 7 h after injection, mice from Group III, IV, and V received 660 nm laser irradiation (1 W/cm^2, 15 min). After treatments, the tumor volumes and mouse body weights were measured every other day during 15-day study duration. Tumors were collected at second day and major organs collected at the fifteen days post treatment for H&E staining. The tumor volumes were calculated according to the following formula: width^2 × length/2.

ASSOCIATED CONTENT

Supporting Information.

The Supporting Information is available free of charge on the ACS Publications website. General information about materials, experimental details, including

detailed synthetic procedures, ^{1}H-NMR, ^{13}C NMR, MS, and UV-visible absorption spectra of the compounds, and supplemental in vitro and in vivo characterization.

AUTHOR INFORMATION

Corresponding Author

xbzhang@hnu.edu.cn

Author Contributions

‡*These authors contributed equally.*

Notes

The authors declare no competing financial interest.

ACKNOWLEDGMENT

This work was supported by the National Natural Science Foundation of China (Grants 21675043，21890744，51872088，21804039).

REFERENCES

1. Li, S. Z.; Yuan, S.; Zhao, Q.; Wang, B.; Wang, X. Y.; Li, K., Quercetin Enhances Chemotherapeutic Effect of Doxorubicin Against Human Breast Cancer Cells While Reducing Toxic Side Effects of It. *Biomed. Pharmacother.* **2018,** *100*, 441-447.

2. Lovell, J. F.; Liu, T. W.; Chen, J.; Zheng, G., Activatable Photosensitizers for Imaging and Therapy. *Chem. Rev.* **2010,** *110* (5), 2839-2857.

3. Wang, H.; Agarwal, P.; Zhao, S.; Yu, J.; Lu, X.; He, X., A Biomimetic Hybrid Nanoplatform for Encapsulation and Precisely Controlled Delivery of Theranostic Agents. *Nat. Commun.* **2015,** *6*, 10081-10093.

4. Shi, B.; Yan, Q.; Tang, J.; Xin, K.; Zhang, J.; Zhu, Y.; Xu, G.; Wang, R.; Chen, J.; Gao, W.; Zhu, T.; Shi, J.; Fan, C.; Zhao, C.; Tian, H., Hydrogen Sulfide-Activatable Second Near-Infrared Fluorescent Nanoassemblies for Targeted Photothermal Cancer Therapy. *Nano. Lett.* **2018,** *18* (10), 6411-6416.

5. Fan, W.; Huang, P.; Chen, X., Overcoming The Achilles' Heel of Photodynamic Therapy. *Chem. Soc. Rev.* **2016,** *45* (23), 6488-6519.

6. Liu, C.; Zhang, R.; Zhang, W.; Liu, J.; Wang, Y. L.; Du, Z.; Song, B.; Xu, Z. P.; Yuan, J., "Dual-Key-and-Lock" Ruthenium Complex Probe for Lysosomal Formaldehyde in Cancer Cells and Tumors. *J. Am. Chem. Soc.* **2019**, 141 (21), 8462-8472.

7. Wang, N.; Yu, X.; Zhang, K.; Mirkin, C. A.; Li, J., Upconversion Nanoprobes for the Ratiometric Luminescent Sensing of Nitric Oxide. *J. Am. Chem. Soc.* **2017,** *139* (36), 12354-12357.

8. Gong, F.; Cheng, L.; Yang, N.; Jin, Q.; Tian, L.; Wang, M.; Li, Y.; Liu, Z., Bimetallic Oxide MnMoOX Nanorods for In Vivo Photoacoustic Imaging of GSH and Tumor-Specific Photothermal Therapy. *Nano. Lett.* **2018,** *18* (9), 6037-6044.

9. Chen, Q.; Liang, C.; Sun, X.; Chen, J.; Yang, Z.; Zhao, H.; Feng, L.; Liu, Z., H_2O_2-Responsive Liposomal Nanoprobe for Photoacoustic Inflammation Imaging

and Tumor Theranostics *via* In Vivo Chromogenic Assay. *Proc. Natl. Acad. Sci. U S A* **2017,** *114* (21), 5343-5348.

10. Zhao, X.; Yang, C. X.; Chen, L. G.; Yan, X. P., Dual-Stimuli Responsive and Reversibly Activatable Theranostic Nanoprobe for Precision Tumor-Targeting and Fluorescence-Guided Photothermal Therapy. *Nat. Commun.* **2017,** *8*, 14998-15007.

11. Tian, J.; Ding, L.; Xu, H. J.; Shen, Z.; Ju, H.; Jia, L.; Bao, L.; Yu, J. S., Cell-Specific and pH-Activatable Rubyrin-Loaded Nanoparticles for Highly Selective Near-Infrared Photodynamic Therapy Against Cancer. *J. Am. Chem. Soc.* **2013,** *135* (50), 18850-18858.

12. Shen, Y. Z.; Tian, Q.; Sun, Y. D.; Xu, J. J.; Ye, D. J.; Chen, H. Y., ATP-Activatable Photosensitizer Enables Dual Fluorescence Imaging and Targeted Photodynamic Therapy of Tumor. *Anal.Chem.* **2017,** *89* (24), 13610-13617.

13. Wu, L.; Sun, Y.; Sugimoto, K.; Luo, Z.; Ishigaki, Y.; Pu, K.; Suzuki, T.; Chen, H. Y.; Ye, D., Engineering of Electrochromic Materials as Activatable Probes for Molecular Imaging and Photodynamic Therapy. *J. Am. Chem. Soc.* **2018,** *140* (47), 16340-16352.

14. Zhao, J.; Gao, J.; Xue, W.; Di, Z.; Xing, H.; Lu, Y.; Li, L., Upconversion Luminescence-Activated DNA Nanodevice for ATP Sensing in Living Cells. *J. Am. Chem. Soc.* **2018,** *140* (2), 578-581.

15. Cheng, H. B.; Zhang, Y. M.; Liu, Y.; Yoon, J. Y., Turn-On Supramolecular Host-Guest Nanosystems as Theranostics for Cancer. *Chem* **2019,** *5* (3), 553-574.

16. Li, X.; Kim, C.; Lee, S.; Lee, D.; Chung, H.-M.; Kim, G.; Heo, S.-H.; Kim, C.; Hong, K.-S.; Yoon, J., Nanostructured Phthalocyanine Assemblies with Protein-Driven Switchable Photoactivities for Biophotonic Imaging and Therapy. *J. Am. Chem. Soc.* **2017,** *139* (31), 10880-10886.

17. Ma, Y.; Li, X.; Li, A.; Yang, P.; Zhang, C.; Tang, B., H_2S-Activable MOF Nanoparticle Photosensitizer for Effective Photodynamic Therapy Against Cancer with Controllable Singlet-Oxygen Release. *Angew. Chem. Int. Ed.* **2017,** *56* (44), 13752-13756.

18. Zhen, X.; Zhang, J.; Huang, J.; Xie, C.; Miao, Q.; Pu, K., Macrotheranostic Probe with Disease-Activated Near-Infrared Fluorescence, Photoacoustic, and Photothermal Signals for Imaging-Guided Therapy. *Angew. Chem. Int. Ed.* **2018,** *57* (26), 7804-7808.

19. Li, X.; Lee, S.; Yoon, J., Supramolecular Photosensitizers Rejuvenate Photodynamic Therapy. *Chem. Soc. Rev.* **2018,** *47* (4), 1174-1188.

20. Tang, Y.; Li, Y.; Hu, X.; Zhao, H.; Ji, Y.; Chen, L.; Hu, W.; Zhang, W.; Li, X.; Lu, X.; Huang, W.; Fan, Q., "Dual Lock-and-Key"-Controlled Nanoprobes for Ultrahigh Specific Fluorescence Imaging in the Second Near-Infrared Window. *Adv. Mater.* **2018,** *30* (31), 1801140-1801149.

21. Ren, K.; Liu, Y.; Wu, J.; Zhang, Y.; Zhu, J.; Yang, M.; Ju, H., A DNA Dual Lock-and-Key Strategy for Cell-Subtype-Specific siRNA Delivery. *Nat. Commun.* **2016,** *7*, 13580-13590.

22. Reinhardt, C. J.; Zhou, E. Y.; Jorgensen, M. D.; Partipilo, G.; Chan, J., A Ratiometric Acoustogenic Probe for In Vivo Imaging of Endogenous Nitric Oxide. *J. Am. Chem. Soc.* **2018,** *140* (3), 1011-1018.

23. Miao, Q. Q.; Lyu, Y.; Ding, D.; Pu, K., Semiconducting Oligomer Nanoparticles as an Activatable Photoacoustic Probe with Amplified Brightness for In Vivo Imaging of pH. *Adv. Mater.* **2016,** *28* (19), 3662-3668.

24. Liu, Y.; Bhattarai, P.; Dai, Z.; Chen, X., Photothermal Therapy and Photoacoustic Imaging via Nanotheranostics in Fighting Cancer. *Chem. Soc. Rev.* **2019,** *48* (7), 2053-2108.

25. Zhang, J.; Smaga, L. P.; Satyavolu, N. S. R.; Chan, J.; Lu, Y., DNA Aptamer-Based Activatable Probes for Photoacoustic Imaging in Living Mice. *J. Am. Chem. Soc.* **2017,** *139* (48), 17225-17228.

26. Zhang, J.; Zhen, X.; Upputuri, P. K.; Pramanik, M.; Chen, P.; Pu, K., Activatable Photoacoustic Nanoprobes for In Vivo Ratiometric Imaging of Peroxynitrite. *Adv. Mater.* **2017,** *29* (6), 1604764-1604772.

27. Wang, W.; Satyavolu, N. S. R.; Wu, Z.; Zhang, J. R.; Zhu, J. J.; Lu, Y., Near‐Infrared Photothermally Activated DNAzyme–Gold Nanoshells for Imaging Metal Ions in Living Cells. *Angew. Chem. Inter. Ed.* **2017,** *56* (24), 6798-6802.

28. Wang, D.; Lee, M. M. S.; Xu, W.; Shan, G.; Zheng, X.; Kwok, R. T. K.; Lam, J. W. Y.; Hu, X.; Tang, B. Z., Boosting Non-Radiative Decay to Do Useful Work: Development of a Multi-Modality Theranostic System from an AIEgen. *Angew. Chem. Int. Ed.* **2019,** *58* (17), 5628-5632.

29. Liu, S.; Zhou, X.; Zhang, H.; Ou, H.; Lam, J. W. Y.; Liu, Y.; Shi, L.; Ding, D.; Tang, B. Z., Molecular Motion in Aggregates: Manipulating TICT for Boosting Photothermal Theranostics. *J. Am. Chem. Soc.* **2019,** *141* (13), 5359-5368.

30. Yang, Z.; Dai, Y.; Yin, C.; Fan, Q.; Zhang, W.; Song, J.; Yu, G.; Tang, W.; Fan, W.; Yung, B. C.; Li, J.; Li, X.; Li, X.; Tang, Y.; Huang, W.; Song, J.; Chen, X., Activatable Semiconducting Theranostics: Simultaneous Generation and Ratiometric Photoacoustic Imaging of Reactive Oxygen Species In Vivo. *Adv. Mater.* **2018,** *30* (23), 1707509-1707517.

31. Tang, W.; Yang, Z.; Wang, S.; Wang, Z.; Song, J.; Yu, G.; Fan, W.; Dai, Y.; Wang, J.; Shan, L.; Niu, G.; Fan, Q.; Chen, X., Organic Semiconducting Photoacoustic Nanodroplets for Laser-Activatable Ultrasound Imaging and Combinational Cancer Therapy. *ACS Nano* **2018,** *12* (3), 2610-2622.

32. Jiang, Y.; Upputuri, P. K.; Xie, C.; Zeng, Z.; Sharma, A.; Zhen, X.; Li, J.; Huang, J.; Pramanik, M.; Pu, K., Metabolizable Semiconducting Polymer

Nanoparticles for Second Near ‐ Infrared Photoacoustic Imaging. *Adv. Mater.* **2019,** *31* (11), 1808166-1808175.

33. Li, J.; Pu, K., Development of Organic Semiconducting Materials for Deep-Tissue Optical Imaging, Phototherapy and Photoactivation. *Chem. Soc. Rev.* **2019,** *48* (1), 38-71.

34. Huang, X.; Song, J.; Yung, B. C.; Huang, X.; Xiong, Y.; Chen, X., Ratiometric Optical Nanoprobes Enable Accurate Molecular Detection and Imaging. *Chem. Soc. Rev.* **2018,** *47* (8), 2873-2920.

35. Garcia-Ortiz, A.; Serrador, J. M., Nitric Oxide Signaling in T Cell-Mediated Immunity. *Trends. Mol. Med.* **2018,** *24* (4), 412-427.

36. Diakos, C. I.; Charles, K. A.; McMillan, D. C.; Clarke, S. J., Cancer-Related Inflammation and Treatment Effectiveness. *Lancet. Oncol.* **2014,** *15* (11), 493-503.

37. Hanahan, D.; Weinberg, R. A., Hallmarks of Cancer: The Next Generation. *Cell* **2011,** *144* (5), 646-674.

38. Grivennikov, S. I.; Greten, F. R.; Karin, M., Immunity, Inflammation, and Cancer. *Cell* **2010,** *140* (6), 883-899.

39. Wang, F.; Yu, S.; Xu, Z.; Li, L.; Dang, Y.; Xu, X.; Luo, Y.; Cheng, Z.; Yu, H.; Zhang, W.; Zhang, A.; Ding, C., Acid-Promoted D-A-D Type Far-Red Fluorescent Probe with High Photostability for Lysosomal Nitric Oxide Imaging. *Anal. Chem.* **2018,** *90* (13), 7953-7962.

40. Qian, G.; Dai, B.; Luo, M.; Yu, D.; Zhan, J.; Zhang, Z.; Ma, D.; Wang, Z. Y., Band Gap Tunable, Donor−Acceptor−Donor Charge-Transfer Heteroquinoid-Based Chromophores: Near Infrared Photoluminescence and Electroluminescence. *Chem. Mater.* **2008,** *20* (19), 6208-6216.

41. Huo, Y.; Miao, J.; Han, L.; Li, Y.; Li, Z.; Shi, Y.; Guo, W., Selective and Sensitive Visualization of Endogenous Nitric Oxide in Living Cells and Animals

by A Si-Rhodamine Deoxylactam-Based Near-Infrared Fluorescent Probe. *Chem. Sci.* **2017,** *8* (10), 6857-6864.

Table of Contents